Biochemistry

 Volume 37, Number 25 June 23, 1998

Accelerated Publications

Solution Structure of the Transmembrane H^+-Transporting Subunit c of the F_1F_o ATP Synthase†

Mark E. Girvin,*,‡,§ Vinit K. Rastogi,§ Frits Abildgaard,|| John L. Markley,|| and Robert H. Fillingame*,‡

Department of Biomolecular Chemistry, University of Wisconsin Medical School, and Biochemistry Department, University of Wisconsin, Madison, Wisconsin 53706, and Biochemistry Department, Albert Einstein College of Medicine, 1300 Morris Park Avenue, Bronx, New York 10461

Received March 4, 1998; Revised Manuscript Received April 22, 1998

ABSTRACT: Subunit c is the H^+-translocating component of the F_1F_o ATP synthase complex. H^+ transport is coupled to conformational changes that ultimately lead to ATP synthesis by the enzyme. The properties of the monomeric subunit in a single-phase solution of chloroform−methanol−water (4:4:1) have been shown to mimic those of the protein in the native complex. Triple resonance NMR experiments were used to determine the complete structure of monomeric subunit c in this solvent mixture. The structure of the protein was defined by >2000 interproton distances, 64 $^3J_{N\alpha}$, and 43 hydrogen-bonding NMR-derived restraints. The root mean squared deviation for the backbone atoms of the two transmembrane helices was 0.63 Å. The protein folds as a hairpin of two antiparallel helical segments, connected by a short structured loop. The conserved Arg41-Gln42-Pro43 form the top of this loop. The essential H^+-transporting Asp61 residue is located at a slight break in the middle of the C-terminal helix, just prior to Pro64. The C-terminal helix changes direction by 30 ± 5° at the conserved Pro64. In its protonated form, the Asp61 lies in a cavity created by the absence of side chains at Gly23 and Gly27 in the N-terminal helix. The shape and charge distribution of the molecular surface of the monomeric protein suggest a packing arrangement for the oligomeric protein in the F_o complex, with the front face of one monomer packing favorably against the back face of a second monomer. The packing suggests that the proton (cation) binding site lies between packed pairs of adjacent subunit c.

The F_1F_o ATP synthase uses a transmembrane electrochemical H^+ gradient to drive the synthesis of ATP from ADP and P_i. H^+ translocation through the membrane-spanning F_o portion of the enzyme drives ATP formation at catalytic sites distantly located in the extrinsic, F_1 sector of the enzyme. The crystal structure of the $\alpha_3\beta_3\gamma$ portion of F_1 shows three α and three β subunits alternating at the

† This study was supported by U.S. Public Health Service Grants GM23105 (R.H.F.) and GM55371 (M.E.G.). The National Magnetic Resonance Facility at Madison, supported by NIH Grant R02301, was used in this study. Equipment in the facility was purchased with funds from the University of Wisconsin, the NSF Biological Instrumentation Program (Grant DMB8415048), the NIH Biomedical Research Technology Program (RR02301), the NIH Shared Instrumentation Program (Grant RR02781), and the U.S. Department of Agriculture. The AECOM Structural NMR Resource, supported by Albert Einstein College of Medicine and the NSF Academic Research Infrastructure Program (DBI9601607), was also used in this study.

* Authors to whom correspondence should be addressed. M.E.G.: telephone, (718) 430-2025; fax, (718) 430-8565; e-mail, girvin@aecom.yu.edu. R.H.F.: telephone, (608) 262-1439; fax, (608) 262-5253; e-mail, filingam@macc.wisc.edu.

‡ University of Wisconsin Medical School.

§ Albert Einstein College of Medicine.

|| University of Wisconsin.

S0006-2960(98)00511-X CCC: $15.00
Published on Web 06/05/1998

periphery of a spherical structure with a centrally located γ subunit interacting asymmetrically with the three β catalytic subunits (*1*). The γ subunit was subsequently shown to rotate with respect to the β subunits during the course of catalysis (*2*−*4*), substantiating Boyer's alternating sites hypothesis (*5*). Rotation of the γ subunit within the $\alpha_3\beta_3$ hexamer of F_1 must be driven by H^+ translocation through F_o. Subunits δ and ϵ of F_1 are involved in coupling H^+ transport to ATP synthesis, and NMR[1] structures of the isolated subunits have been reported (*6*, *7*). The structure of the membrane spanning F_o sector is unknown. It is composed of three types of subunits in an $a_1b_2c_{10-12}$ stoichiometry (*8*, *9*). Subunit c plays a direct role in coupling H^+ translocation to conformational changes in F_1 driving ATP synthesis. It is thought to fold through the membrane as a hairpin of antiparallel, hydrophobic α-helices connected by a polar loop. An essential carboxyl group at the center of the membrane (Asp61 in *Escherichia coli*) serves as the H^+ binding site (*9*). H^+ binding and release at Asp61, and a resultant conformational change in the loop region of the protein, are thought to drive rotation of the γ subunit and release of ATP product from F_1 (*9*). An atomic resolution structure of subunit c is required to understand this process. We have shown by homonuclear NMR experiments that monomeric subunit c folds as a hairpin of two antiparallel helical segments in a single-phase chloroform−methanol−water (4:4:1) mixture (*10*, *11*). Further, features of the protein seen in the native F_o complex are retained in this solvent mixture (*12*, *13*). Determination of the complete structure of the protein by homonuclear methods was not possible, owing to the extensive resonance overlap in this largely helical protein which is highly enriched in hydrophobic amino acids. To overcome these obstacles, we undertook a heteronuclear NMR study of $^{13}C^{15}N$ labeled subunit c. The complete structure of monomeric subunit c is reported here.

EXPERIMENTAL PROCEDURES

Sample Preparation. Wild-type *E. coli* subunit c was prepared as described (*11*) from strain MEG119 [plasmid pCP35 (*14*) transformed into an Asn^+ derivative of strain ER (*15*)]. Uniform $^{13}C^{15}N$ labeling was achieved by growth of cells on 15 mM $^{15}NH_4Cl$ and 8.9 mM [^{13}C]glucose as the sole nitrogen and carbon sources. NMR samples were 0.6 mL of 2.5−3 mM subunit c in 4:4:1 $CDCl_3-CD_3OH-H_2O$ plus 50 mM NaCl, pH 5.

NMR Spectroscopy. NMR experiments were carried out on Bruker DMX-500 and DRX-600 spectrometers at 300 K. All experiments made use of pulsed field gradients for coherence selection and artifact suppression (*16*, *17*). Sensitivity enhancement schemes (*17*, *18*) were used in the pulse programs wherever possible. Quadrature detection in the indirect dimensions was via States−TPPI (*19*).

Intraresidue backbone resonances were identified from 3D HNCO (*20*), HCACO (*21*), HNCACB (*22*), and $^1H^{15}N$ TOCSY-HSQC (*23*) experiments. Sequential assignments were derived by correlating these intraresidue assignments with the interresidue cross peaks observed in CBCA(CO)-NH (*24*), C(CO)NH, and H(CCO)NH (*25*) spectra. Aliphatic side chain ^1H and ^{13}C resonances were assigned from HCCH-COSY and HCCH-TOCSY (*26*) and $^1H^{13}C$ CT-HSQC (*27*) data. Aromatic ^1H and ^{13}C were identified in a 3D ^1H-TOCSY-CT-HMQC (*28*).

Distance constraints were derived from NOEs observed in $^1H^{13}C$ and $^1H^{15}N$ NOESY-HSQC (*29*) spectra, with mixing times of 150 ms. NOEs from aromatic side chain protons were detected in a $^1H^{13}C$ NOESY-CT-HSQC experiment. H^NH^α coupling constants were measured in an HNCA-*J* experiment (*30*). N^H-N^D exchange was measured by diluting the sample 3-fold with perdeuterated solvent and recording a series of 10 min $^1H^{15}N$ HSQC experiments over a period from 15 min to 36 h.

Spectral data were processed using nmrPipe (*31*). The data in all indirect dimensions were extended by linear prediction and zero-filling. Internal tetramethylsilane was used to reference ^1H chemical shift directly and ^{13}C and ^{15}N indirectly (*32*). The program PIPP (D. Garrett, NIH) was used for automated peak picking. Manual checks and additional manual peak selections were done within nmrDraw.

Structure Calculation, Refinement, and Evaluation. Fifty initial structures were calculated by simulated annealing using torsion angle dynamics as implemented in the program DYANA (*33*). A total of 2008 NOE-derived distance restraints were used as input for the initial structure calculations. NOEs were characterized as strong, medium, or weak, with corresponding upper distance limits of 2.8, 3.5, or 5.0 Å. These upper limits were increased for restraints involving protons which were not stereospecifically assigned (*34*). The best initial structures were used to assign dihedral anglerestraints, based on the 64 H^NH^α coupling constants, and hydrogen bond restraints for the 43 H^N that exchanged with half-times greater than 12 h. These additional restraints were combined with the initial NOE restraints to refine the 20 best structures using X-PLOR 3.851 (*35*). A simulated annealing protocol was used for the refinement, with a maximum simulation temperature of 750 K. The ten best final structural models were evaluated using AQUA and PROCHECK-NMR (*36*). The final atomic coordinates have been deposited as entry 1a91 at the Protein Data Bank.

RESULTS

The dispersion of chemical shifts in doubly labeled subunit c was significantly smaller than that seen for water-soluble proteins but was comparable to that observed for other membrane proteins (e.g., *37*, *38*). Although the amide $^1H^{15}N$ cross peak dispersion was limited (Figure 1A), all 76 backbone amides were assigned in the present study. The additional resolution from ^{13}C labeling was sometimes limited because of degeneracy in the ^{13}C chemical shifts, e.g., for the C^α and C^β of the 12 Leu side chain resonances (Figure 1B). A larger number of experiments and larger data matrices were thus required to make the assignments for subunit c than typically would be used for proteins of this size. With the additional data it was possible to assign all backbone and nearly all side chain ^1H, ^{13}C, and ^{15}N resonances.

Resonance Assignments. The 3D HNCO was used to resolve all backbone amides which were degenerate in 2D

[1] Abbreviations: $^3J_{N\alpha}$, three-bond H^NH^α coupling constants; CT, constant time; DCCD, *N*,*N*′-dicyclohexylcarbodiimide; HSQC, heteronuclear single-quantum correlation; NMR, nuclear magnetic resonance; NOE, nuclear Overhauser effect; NOESY, NOE spectroscopy; RMS, root mean squared; TOCSY, total correlation spectroscopy.

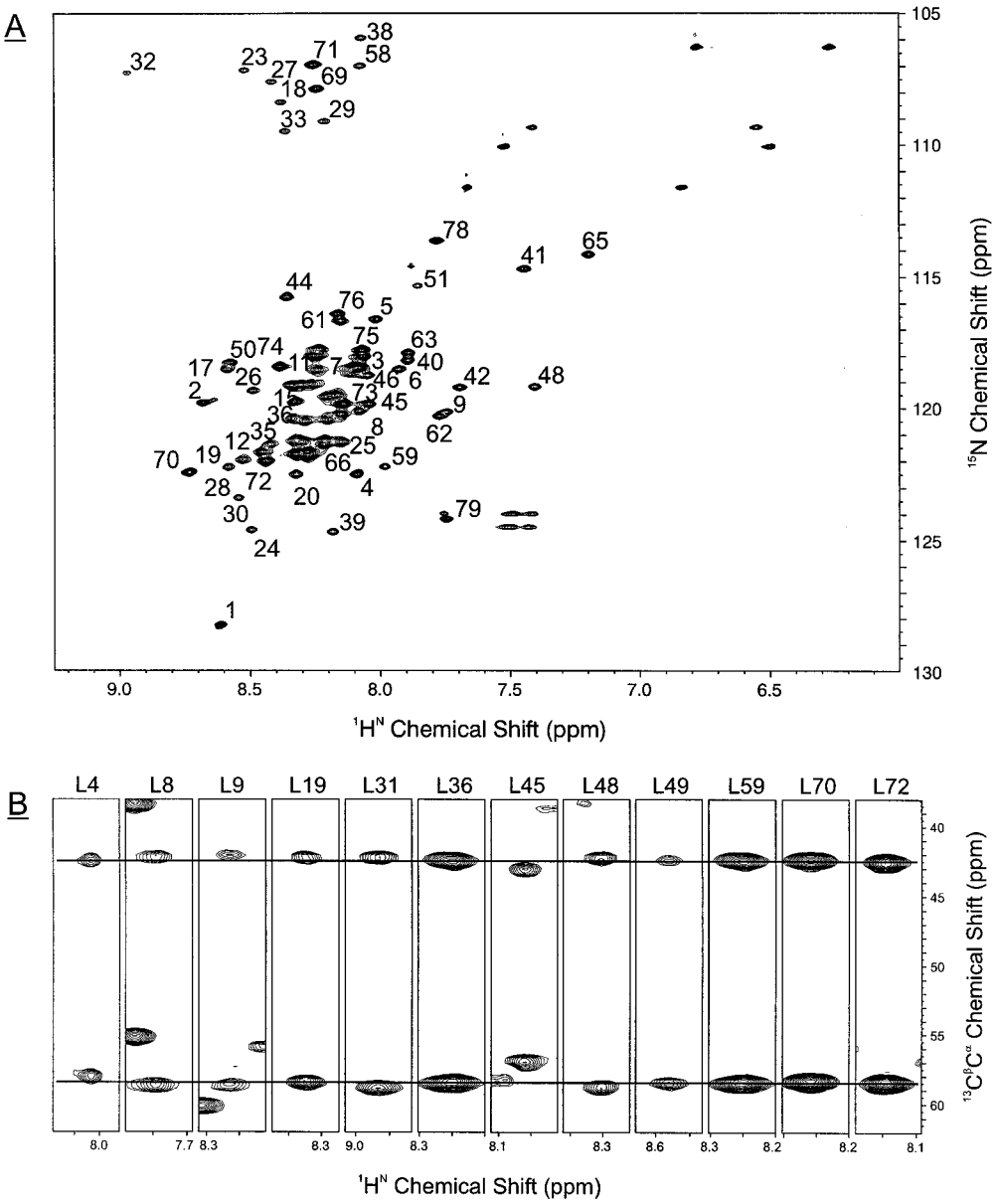

FIGURE 1: ^{1}H, ^{15}N, and ^{13}C spectral resolution and degeneracy in subunit c. (A) 2D ^{1}H^{15}N HSQC spectrum of 2.5 mM subunit c at 300 K. All 76 backbone amide cross peaks are shown, and those outside the most congested regions are labeled with their assignments (B) Strips showing the ^{13}C$^{\alpha}$ and ^{13}C$^{\beta}$ cross peaks for the 12 Leu side chains of subunit c, taken from the 3D CBCA(CO)NH experiment. Reference lines are drawn at 58.5 and 42.5 ppm to illustrate the similarity of ^{13}C$^{\alpha}$ and ^{13}C$^{\beta}$ chemical shifts.

experiments. The C$^{\alpha}$/C$^{\beta}$ and H$^{\alpha}$/H$^{\beta}$ within each residue were correlated with the backbone ^{1}H^{15}N using the HNCACB and TOCSY-HSQC experiments. Side chain ^{1}H and ^{13}C were then identified in the HCCH-COSY and HCCH-TOCSY data sets, using the C$^{\alpha}$C$^{\beta}$ and H$^{\alpha}$H$^{\beta}$ chemical shifts as starting points. The three Pro were identified from new sets of ^{1}H^{13}C α, β, and γ resonances in the HCCH-TOCSY and HCCH-COSY experiments. Most residue types were distinguishable at this point. Sequential assignments were made by correlating C$^{\alpha}$/C$^{\beta}$ and H$^{\alpha}$/H$^{\beta}$ side chain resonances of the previous ($i - 1$) residue observed in the CBCA(CO)NH, C(CO)NH, and H(CCO)NH experiments with the identified intraresidue ^{1}H^{15}Ns. A sample series of correlated intraresidue TOCSY-HSQC cross peaks along with the corresponding (i,$i - 1$) interresidue cross peaks from an H(CCO)NH spectrum is shown in Figure 2 for the sequence from Ala25 to Gly29. Additional data from the NOESY experiments were used to identify the correct partners when the HN were degenerate. The sets of Tyr and Phe aromatic ^{1}H and ^{13}C were identified in a TOCSY-CT-HMQC experiment and assigned to specific residues from ^{1}H^{13}C NOESY-CT-HSQC data. Full assignments have been deposited at the BMRB (http://www.bmrb.wisc.edu).

Constraints for Structure Calculations. NOEs from all protons to the amide protons were identified in ^{1}H^{15}N NOESY-HSQC spectra. Figure 3A summarizes the backbone NOEs observed for subunit c. As expected, the observed ~475 amide NOEs for most of the protein were those typical of an α-helix. From the amide NOE patterns alone, the protein appeared to be helical from Met1 through Ala40, from Leu45 through Ala62, and from Met65 throughAla77. Secondary ^{13}C$^{\alpha}$ and ^{13}C′ chemical shifts (*39*) were also consistent with these segments of helical secondary structure (Figure 3A). Short distances between ^{13}C-attached protons were detected in ^{1}H^{13}C NOESY-HSQC spectra. A separate ^{1}H^{13}C NOESY-CT-HSQC with pulses optimized for

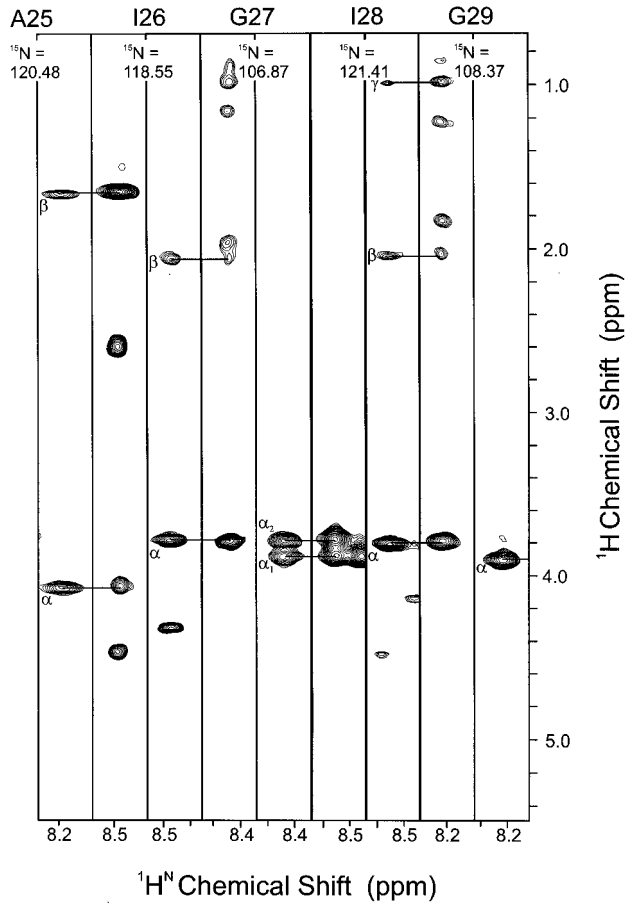

FIGURE 2: Example assignment strips from a pair of intra- and interresidue 3D experiments. Alternating strips of the interresidue H(CCO)NH and the intraresidue TOCSY-HSQC data sets are shown for Ala25 through Gly29. Each pair is shown at the ^{1}H^{15}N position for the intraresidue experiment. From the right, the intraresidue ^{1}H^{15}N−^{1}H$^\alpha$ is shown in the TOCSY-HSQC for Gly29. The next strip to the left shows the Gly29 H(CCO)NH ^{1}H^{15}N interresidue correlation to the Ile28 H$^\alpha$, H$^\beta$, H$^\gamma$, followed by the intraresidue TOCSY-HSQC strip for Ile28 at its own ^{1}H^{15}N, etc., until the Ala25 intraresidue TOCSY-HSQC strip at the far left is reached.

aromatic ^{13}C was required for sensitive observation of the ∼65 NOEs to aromatic protons. Altogether, 15−90 NOE restraints per residue were identified, as illustrated in Figure 3B. The 64 $^3J_{N\alpha}$ coupling constants measured from the HNCA-*J* spectrum were small (2−6 Hz), consistent with helical structure (*40*). Three chain segments were identified as having amide protons that exchanged slowly with solvent (half-times >12 h): Leu8−Gly33, Phe54−Val60, and Ile66−Phe76. Several of these showed no detectable exchange even after 36 h.

Structure Calculation and Description. Structure calculation by torsion angle dynamics followed with refinement by simulated annealing and energy minimization led to the family of structures shown in Figure 4A. The structural models fit the NMR data well, with no violations of experimental distance restraints greater than 0.4 Å. The positions of the backbone and most side chain atoms were well defined by the NMR restraints. The models shown in Figure 4A were superimposed on the basis of the backbone coordinates for residues 10−35 and 50−73. For these residues the backbone atomic RMS deviations were 0.62 Å and were 1.06 Å for all non-hydrogen atoms. The main variation between structures was in the overall curvature of the helical pair. If smaller 15-residue segments along the length were superimposed, the backbone atom RMS deviations dropped to <0.3 Å. Figure 4B shows the improvement observed in the definition of the loop connecting the two helices when superimposed using only residues 35−52. Variation in curvature is almost certainly due to the absence of long-range distance constraints over the ∼60 Å length of this molecule. Structural statistics are presented in Table 1.

Table 1: Statistics for the 10 Final Structural Models

NOE distance restraints (total 2008)	
intraresidue	694
sequential	548
medium	647
interhelix	119
ϕ dihedral angle restraints	64
backbone hydrogen bonds	43
RMSD of atomic coordinates (residues 10−35, 50−73)	
backbone (Å)	0.63
all non-hydrogen (Å)	1.06
deviations from exptl distance restraints	
largest (Å)	0.32
RMS (Å)	0.03
deviations from exptl dihedral angle restraints	
largest (deg)	2.38
RMS (deg)	0.33
Ramachandran plot	
residues in most favored regions	93.0%
residues in additional allowed regions	7.0%
RMSD from ideal geometry	
bond lengths (Å)	0.005
bond angles (deg)	0.679
impropers (deg)	0.516
van der Waals energy[a] (kcal/mol)	−349.2 ± 4.9

[a] Calculated using Amber 4.1 with the amber91 force field (*55*).

The overall structure is most simply described as a helical hairpin with a short connecting loop in the center of the molecule. The very long N-terminal helix extends from Glu2 at one end of the molecule to Ala40 at the beginning of the connecting loop (Figures 4A and 5A). The loop, formed by residues 41−47, places the conserved Arg41, Gln42, and Pro43 residues at the apex of the turn at the top of the structure (Figure 4B). The C-terminal helical domain is composed of two α-helical segments with a slight disruption in secondary structure centered around Asp61 in four of the ten structural models. Standard α-helical geometry is observed for residues 48−58 and 65−77. The H^N exchange rates indicate weaker hydrogen bonding for residues 61−65. The extended N-terminal helix is gently curved by 10−15° over its length, with the largest change centered at Leu19, where a slight bulge is observed. The course of the C-terminal helical domain alters more dramatically with an abrupt 30 ± 5° change in direction beginning at Pro64. The N- and C-terminal helices pack in nearly parallel fashion from the loop to residues 20 and 63. Van der Waals contact is made between the H$^\alpha$ and H$^\beta$ of Ala24 and the H$^\beta$ of Asp61. The main chain atoms of the two helices diverge from each other toward the N- and C-termini due to the change in direction of the C-terminal helix.

The N- and C-terminal helices are in side chain contact over nearly their full length, with contacts between helices extending from Leu9 to Ala39 and Pro47 to Tyr73. The interhelical packing results in an oval-shaped cross section, with flattened surfaces opposite each other. The Asp61 side

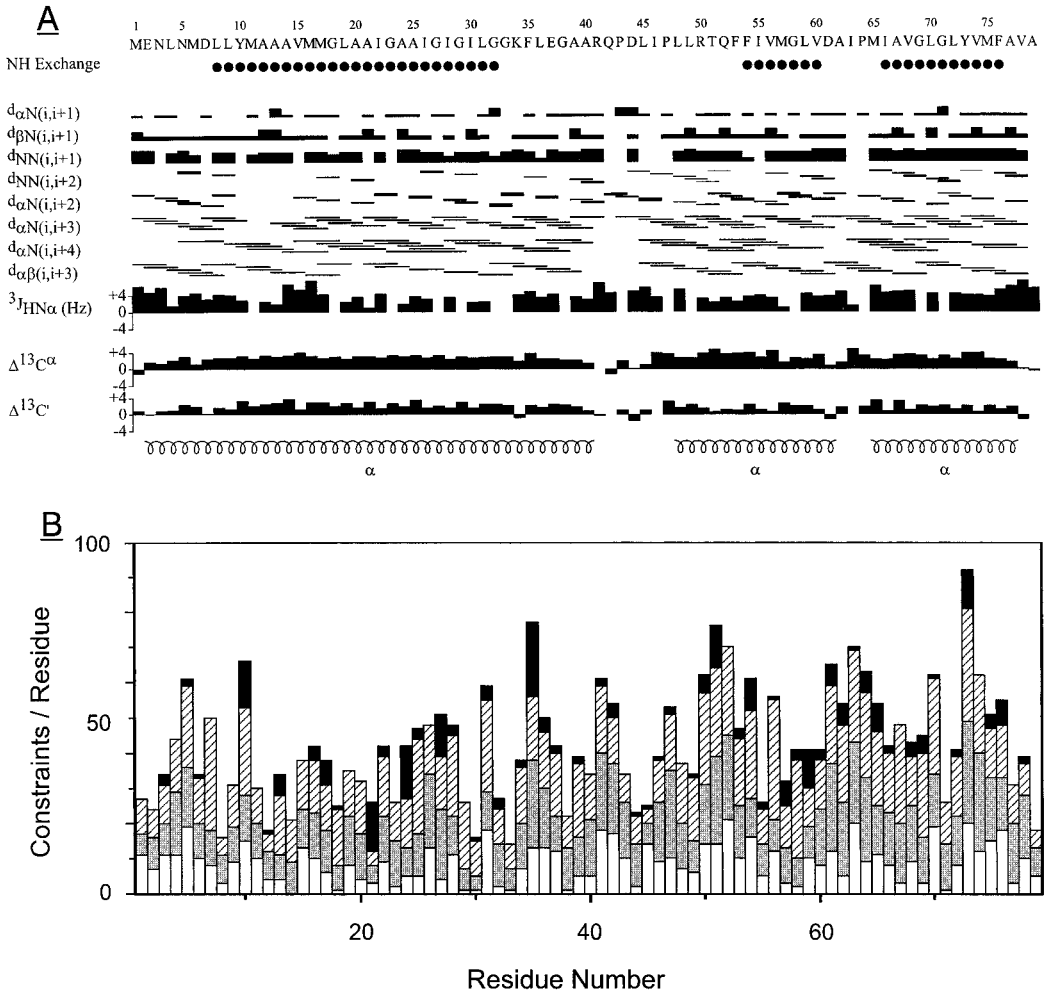

FIGURE 3: Summary of NMR restraints derived for subunit c. (A) Filled circles indicate amide protons with half-times for exchange with solvent greater than 12 h. Horizontal lines identify backbone NOEs, with widths indicating approximate cross peak intensity, $^3J_{N\alpha}$ and secondary shifts of $^{13}C^{\alpha}$ and $^{13}C'$ are also shown. (B) Number of NOE restraints per residue. White bars indicate intraresidue NOEs, light gray bars indicate $i,i+1$ sequential NOEs, hatched bars indicate medium-range NOEs, and black bars indicate long-range NOEs.

chain lies on one flattened surface, which we designate "front", and the Ala24 and Ala62 side chains lie on the opposing "back" surface (Figure 4A). At the N- and C-termini of the protein, the ring of Tyr10 is sandwiched between the rings of Tyr73 and Phe76 on the back surface, with ring centroid−centroid distances being 5.6 ± 0.2 and 4.5 ± 0.2 Å, respectively. At the loop end of the molecule, the Phe35 ring extends between the δ-guanido group of Arg50 and the ring of Phe54 on the front side of the molecule, with centroid distances from the Phe35 ring to Arg50 C^{ξ} and to the Phe54 ring being 5.0 ± 0.6 and 4.0 ± 0.5 Å, respectively. These aromatic packing interactions are in accord with the stabilizing geometries described by Burley and Petsko (*41*). Additional residues make contact at the interhelical packing interface: side chains of Leu9 with Met75 and Ala12 with Leu72 on the front face; side chains of Met16 and Val68 on the front face; Met17 backbone with Met65 side chain on the front face and side chains of Met17 and Ile66 on the back face; Ala20 carbonyl and Asp61 side chain O^{δ}; Ala20 and Met65 side chains on the front face; Ile28 and Leu59 side chains on the back face; side chains of Leu31 with Met57 and Phe54 on the front face; and, just below the loop, side chains of Ala39 with Pro47. Helix−helix interactions appear to be van der Waals in nature. No ion pairing between helices is indicated. The only potential interhelical hydrogen bond involves Asp61.

The functionally essential Asp61 is located in the middle of the C-terminal helix at the point where the helix changes direction. The Asp61 and Ala24 side chains are positioned opposite to each other on opposing flattened surfaces. The Asp61 carboxyl packs close to the Ala20 and Ala24 backbone in a cavity created by the absence of side chains at Gly23, Gly27, and Gly58. In 4 of the 10 conformers, the Asp61 side chain is positioned such that the protonated Asp61 carboxyl could donate a hydrogen bond to the carbonyl of Ala20, with Asp61 O^{δ}−Ala20 carbonyl distances of 3.4 ± 0.2 Å.

DISCUSSION

Monomeric subunit c of the H^+ ATP synthase folds in a compact helix−loop−helix structure in the mixed solvent system used here. The extended antiparallel helices appear to be strongly associated. More than 100 interhelical NOEs were resolved; others existed which could not be assigned unambiguously due to chemical shift degeneracy. The protein folds as predicted from sequence analysis (*42*), with a pair of antiparallel hydrophobic helices connected by a polar loop. The loop residues were shown to be exposed

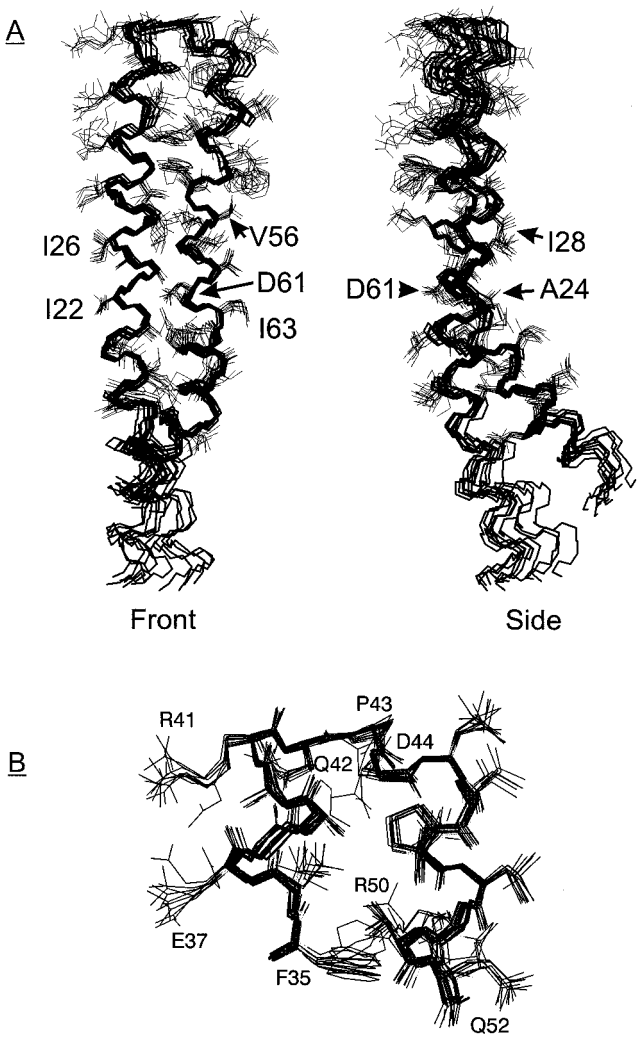

FIGURE 4: Solution structure of subunit c. (A) Backbone traces (bold lines) of the 10 subunit c NMR conformers that best represent the structure, aligned by superimposing the backbone atoms of residues 10−35 and 50−73. The left view is of the "front" face. The right view is rotated by 90° relative to the left. Side chains (lighter lines) are also displayed for residues 10−73. (B) Expansion of the polar loop region. The models were aligned using the backbone coordinates for residues 35−52. All images were produced using MOLMOL (*56*).

on the F_1 binding surface of the membrane by a variety of approaches (*43*−*48*). The alignment of the helices in the NMR structure agrees well with genetic predictions. The Asp61 side chain in the C-terminal helix had been predicted to lie opposite Ala24 in the N-terminal helix (*49*, *50*), and a similar juxtaposition was predicted for Pro64 and Ala20 (*51*). Both of these predictions are borne out in the NMR structure. The folding of subunit c in this mixed solvent system appears to mimic that in the membrane quite well.

The complete structure reported here is quite comparable to the partial structure determined previously using a spin-labeled difference approach (*11*). The earlier partial structure was determined at lower resolution, partly due to uncertainties in the distances estimated from NOEs and partly due to a limited number of long-range restraints. Backbone RMS deviations between the ordered regions of the two structures are ~1.1 Å, with the largest differences arising from differences in the crossing angle of the two helices.

Asp61, the H^+-transporting residue, is centered in the C-terminal helix and is presumably situated near the middle of the membrane bilayer in the native enzyme. Asp61 is protonated at the pH used in this study (*13*). The protonated Asp61 side chain lies in a cavity at the interface between helices, tucked toward the N-terminal helix between Gly23 and Gly27, with Pro64 packing just below on the same surface. The two transmembrane helices are at their minimal cross section at the location of Asp61 due to juxtaposition of small residues in both helices, i.e., Gly23, Ala24, Ala25, and Gly27 in helix 1 and Gly58 and Ala62 in helix 2. The change in direction of the C-terminal helix at Pro64 increases the exposure of the Asp61 carboxyl group. The NMR data indicate that this region of the protein is more flexible than the rest of the C-terminal helix. Ionization of the Asp61 carboxyl is predicted to provoke major structural changes in this region, which ultimately cause changes in the polar loop (*13*). The structure of the ionized form of the protein will be of great interest.

Ala40 through Pro47 form the short loop connecting the two transmembrane segments in the NMR structure. The conserved residues Arg41, Gln42 and Pro43 are known to be involved in the coupling of H^+ translocation through F_o to ATP synthesis on F_1 (*9*). From genetic suppressor analysis (*45*) and cross-linking studies (*46*−*48*), these residues are known to lie at the interface between subunit c and the ϵ and γ subunits of F_1. A change in the orientation of the two helices coming into the loop could alter the loop's structure and hence the structure of the coupling interface between F_o and F_1.

The backbone amide exchange data indicate that the protein folds with three helical elements of stably hydrogen-bonded secondary structure: Leu8−Gly33 in the N-terminal helix and Phe54−Val60 and Ile66−Phe76 in the C-terminal helix. These three helical segments are connected by more weakly H-bonded segments, which are presumably more flexible.[2] The elements of stable helical secondary structure are likely to be retained when the protein changes conformation and simply rearrange with respect to each other. We expect that ionization of Asp61 will induce changes in local structure and a resultant rearrangement of the helical elements to ultimately cause structural changes in the polar loop.

The structure of monomeric subunit c in solution provides hints of how the oligomeric protein may pack in the F_o complex. The majority of the long hydrophobic side chains extend in opposing ridges along the two helices (to the left of the N-terminal helix and to the right of the C-terminal helix in the front orientation of Figure 4A). Gly and Ala predominate in the front and back faces of the interacting helices. An arrangement where the front face of one monomer packs against the back face of another appears likely. The two surfaces are complementary in shape, depressions in one surface complementing protrusions on the other. These surfaces could also interact electrostatically. For example, the positive charge on Arg50 on the front face of one monomer could be balanced by the negative charge on Asp44 on the opposite face of the adjacent monomer. A ribbon diagram of a plausible model for the dimer is shown in Figure 5.

[2] Norwood et al. reported experimental evidence for flexibility in residues 1−8, 35−45, and 76−79 from $^{15}N\{^1H\}$ NOE data for the protein in trifluoroethanol (*52*).

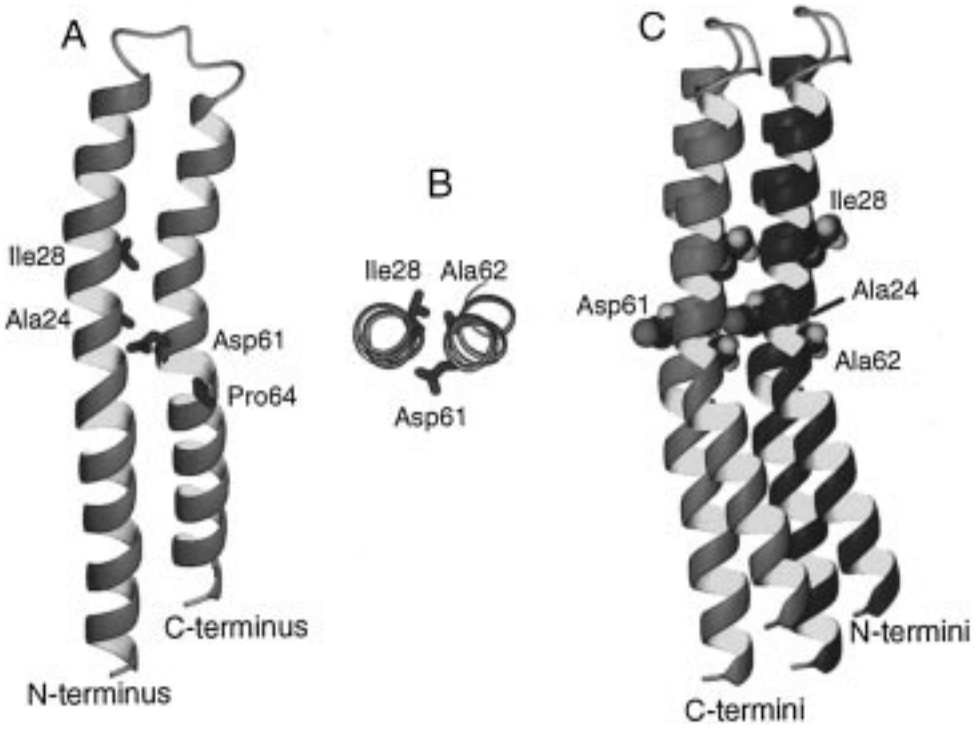

FIGURE 5: Model for the packing of multiple subunit c monomers. (A) Front view of one subunit c monomer. (B) A cross section through the two transmembrane helices shows the relative orientation of the side chains of Ala24, Ile28, Asp61, and Ala62. (C) Two monomers were aligned to give favorable packing and electrostatic interactions. Side chains for Ala24, Ile28, Asp61, and Ala62 are shown.

The arrangement shown in Figure 5 also provides a novel interpretation of several genetic studies. In the functional A24D/D61G double mutant, where the essential Asp was interchanged between positions 61 and 24, the essential carboxyl would end up in the same cavity between subunits regardless of whether it was anchored at backbone position 24 or 61. In DCCD-resistant mutants, the substituted residues at positions 24 or 28 from one monomer would neighbor Asp61 of the adjacent monomer and thereby affect reactivity of the Asp61 carboxyl.[3] Several residues have been identified in which substitutions alter the specificity of the position 61 carboxyl for Li^+ and Na^+ relative to H^+. The Ala62 → Ser substitution in the *E. coli* protein leads to binding of Li^+ (*53*), and Gln and Ser substitutions at positions equivalent to 28 and 62 are required for Na^+ binding by subunit c of *Propiogenium modestum* (*54*). The proposed binding of Na^+ or Li^+ by the combined coordination of the side chain carboxyl at position 61, a side chain hydroxyl at position 62, and a side chain amide at position 28 could not take place within a monomer (Figure 5B). However, the packing arrangement of Figure 5 would place all three side chains in close proximity.

ACKNOWLEDGMENT

We thank Dan Garrett (NIH) for providing PIPP and related peak analysis programs and David P. Goldenberg (University of Utah) for the perl scripts to convert restraints from DYANA format to that used by X-PLOR.

[3] We have noted that the I28T monomeric protein reacts with DCCD at approximately 50% the rate of wild-type protein in chloroform−methanol−water solvent. The differences in reactivity are considerably greater in the intact complex, i.e., approximately 10-fold. The A24S protein isolated from a second DCCD-resistant mutant was as reactive as wild type in chloroform−methanol−water solvent.

SUPPORTING INFORMATION AVAILABLE

A table listing all NMR experiments and parameters and a Ramachandran plot for the final 10 structural models (2 pages). Ordering information is given on any current masthead page.

REFERENCES

1. Abrahams, J. P., Leslie, A. G. W., Lutter, R., and Walker, J. E. (1994) *Nature 370*, 621.
2. Duncan, T. M., Bulygin, V. V., Zhou, Y., Hutcheon, M. L., and Cross, R. L. (1995) *Proc. Natl. Acad. Sci. U.S.A. 92*, 10964.
3. Sabbert, D., Engelbrecht, S., and Junge, W. (1996) *Nature 381*, 623.
4. Noji, H., Yasuda, R., Yoshida, M., and Kinosita, K. J. (1997) *Nature 386*, 299.
5. Boyer, P. (1997) *Annu. Rev. Biochem. 66*, 717.
6. Wilkens, S., Dahlquist, F. W., McIntosh, L. P., Donaldson, L. W., and Capaldi, R. A. (1995) *Nat. Struct. Biol. 2*, 961.
7. Wilkens, S., Dunn, S. D., Chandler, J., Dahlquist, F. W., and Capaldi, R. A. (1997) *Nat. Struct. Biol. 4*, 198.
8. Fillingame, R. H. (1990) in *The Bacteria* (Krulwich, T. A., Ed.) Vol. 12, p 345, Academic Press, New York.
9. Fillingame, R. H. (1997) *J. Exp. Biol. 200*, 217.
10. Girvin, M. E., and Fillingame, R. H. (1993) *Biochemistry 32*, 12167.
11. Girvin, M. E., and Fillingame, R. H. (1995) *Biochemistry 34*, 1635.
12. Girvin, M. E., and Fillingame, R. H. (1994) *Biochemistry 33*, 665.
13. Assadi-Porter, F. M., and Fillingame, R. H. (1995) *Biochemistry 34*, 16186.
14. Fillingame, R. H., Peters, L. K., White, L. K., Mosher, M. E., and Paule, C. R. (1984) *J. Bacteriol. 158*, 1078.
15. Felton, J., Michaelis, S., and Wright, A. (1980) *J. Bacteriol. 142*, 221.
16. Bax, A., and Pochapsky, S. S. (1992) *J. Magn. Reson. 99*, 638.

17. Kay, L. E., Keifer, P., and Saarinen, T. (1992) *J. Am. Chem. Soc. 114*, 10663.
18. Palmer, A. G., Cavanagh, J., Wright, P. E., and Rance, M. (1991) *J. Magn. Reson. 93*, 151.
19. Marion, D., Ikura, M., Tschudin, R., and Bax, A. (1989) *J. Magn. Reson. 85*, 393.
20. Grzesiek, S., and Bax, A. (1992) *J. Magn. Reson. 96*, 432.
21. Powers, R., Gronenborn, A. M., Clore, G. M., and Bax, A. (1991) *J. Magn. Reson. 94*, 209.
22. Wittekind, M., and Mueller, L. (1993) *J. Magn. Reson., Ser. B 101*, 201.
23. Marion, D., Driscoll, P. C., Kay, L. E., Wingfield, P. T., Bax, A., Gronenborn, A. M., and Clore, G. M. (1989) *Biochemistry 28*, 6150.
24. Grzesiek, S., and Bax, A. (1992) *J. Am. Chem. Soc. 114*, 6291.
25. Grzesiek, S., Anglister, J., and Bax, A. (1993) *J. Magn. Reson., Ser. B 101*, 114.
26. Kay, L. E., Xu, G. Y., Singer, A. U., Muhandiram, R., and Forman-Kay, J. D. (1993) *J. Magn. Reson., Ser. B 101*, 333.
27. Vuister, G. W., and Bax, A. (1992) *J. Magn. Reson. 98*, 428.
28. Zerbe, O., Szyperski, T., Ottiger, M., and Wüthrich, K. (1996) *J. Biomol. NMR 7*, 99.
29. Zhang, O., Kay, L. E., Olivier, J. P., and Forman-Kay, J. D. (1994) *J. Biomol. NMR 4*, 845.
30. Seip, S., Balbach, J., and Kessler, H. (1944) *J. Magn. Reson., Ser. B 104*, 172.
31. Delaglio, F., Grzesiek, S., Vuister, G. W., Zhu, G., Pfeifer, J., and Bax, A. (1995) *J. Biomol. NMR 6*, 277.
32. Wishart, D. S., Bigam, C. G., Yao, J., Abildgaard, F., Dyson, H. J., Oldfield, E., Markley, J. L., and Sykes, B. D. (1995) *J. Biomol. NMR 6*, 135.
33. Güntert, P., Mumenthaler, C., and Wüthrich, K. (1997) *J. Mol. Biol. 273*, 283.
34. Wüthrich, K. (1986) *NMR of Proteins and Nucleic Acids*, Wiley, New York.
35. Brünger, A. T. (1993) *X-PLOR Version 3.1: A System for X-ray Crystallography and NMR*, Yale University Press, New Haven, CT.
36. Laskowski, R. A., Rullmann, J. A. C., MacArthur, M. W., Kaptein, R., and Thornton, J. M. (1996) *J. Biomol. NMR 8*, 477.
37. Papavoine, C. H. M., Aelen, J. M. A., Konigs, R. N. H., Hilbers, C. W., and Van de Ven, J. M. 91995) *Eur. J. Biochem. 232*, 490.
38. Williams, K. A., Farrow, N. A., Deber, C. M., and Kay, L. E. (1996) *Biochemistry 35*, 5145.
39. Wishart, D. S., Sykes, B. D., and Richards, F. M. (1991) *J. Mol. Biol. 222*, 311.
40. Vuister, G. W., and Bax, A. (1993) *J. Am. Chem. Soc. 115*, 7772.
41. Burley, S. K., and Petsko, G. A. (1985) *Science 229*, 23.
42. Hoppe, J., and Sebald, W. (1981) *Curr. Top. Bioenerg. 12*, 1.
43. Girvin, M. E., Hermolin, J., Pottorf, R., and Fillingame, R. H. (1989) *Biochemistry 28*, 4340.
44. Hensel, M., Deckers-Hebestreit, G., Schmid, R., and Altendorf, K. (1990) *Biochim. Biophys. Acta 1016*, 63.
45. Zhang, Y., Oldenburg, M., and Fillingame, R. H. (1994) *J. Biol. Chem. 269*, 10221.
46. Zhang, Y., and Fillingame, R. H. (1995) *J. Biol. Chem. 270*, 24609.
47. Watts, S. D., Zhang, Y., Fillingame, R. H., and Capaldi, R. A. (1995) *FEBS Lett. 368*, 235.
48. Watts, S. D., Tang, C., and Capaldi, R. A. (1996) *J. Biol. Chem. 271*, 28341.
49. Miller, M. J., Oldenburg, M., and Fillingame, R. H. (1990) *Proc. Natl. Acad. Sci. U.S.A. 87*, 4900.
50. Fillingame, R. H., Oldenburg, M., and Fraga, D. (1991) *J. Biol. Chem. 266*, 20934.
51. Fimmel, A. L., Jans, D. A., Langman, L., James, L. B., Ash, G. R., Downie, J. A., Senior, A. E., Gibson, F., and Cox, G. B. (1983) *Biochem. J. 213*, 451.
52. Norwood, T. J., Crawford, D. A., Steventon, M. E., Driscoll, P. C., and Campbell, I. D. (1992) *Biochemistry 31*, 6285.
53. Zhang, Y., and Fillingame, R. H. (1995) *J. Biol. Chem. 270*, 87.
54. Kaim, G., Wehrle, F., Gerike, U., and Dimroth, P. (1997) *Biochemistry 36*, 9185.
55. Pearlman, D. A., Case, D. A., Caldwell, J. W., Ross, W. S., Cheatham, T. E. I., Ferguson, D. M., Seibel, G. L., Singh, U. C., Weiner, P. K., and Kollman, P. A. (1995) *AMBER 4.1*, University of California, San Francisco.
56. Koradi, R., Billeter, M., and Wüthrich, K. (1996) *J. Mol. Graphics 14*, 51.

BI980511M